# SIGNAL AND NOISE ANALYSIS OF LARGE MICROWAVE FRONT-ENDS BY THE INEXACT-NEWTON HARMONIC-BALANCE TECHNIQUE

Vittorio RIZZOLI (1), Franco MASTRI (2), and Claudio CECCHETTI (3)

(1) Dipartimento di Elettronica, Informatica e Sistemistica, University of Bologna, Villa Griffone, 40044 Pontecchio Marconi, Bologna, ITALY
(2) Dipartimento di Ingegneria Elettrica, University of Bologna, Viale Risorgimento 2, 40136 Bologna, ITALY
(3) Fondazione Ugo Bordoni, Villa Griffone, 40044 Pontecchio Marconi, Bologna, ITALY

## ABSTRACT

The analysis of complex front-ends containing many nonlinear devices and supporting signal waveforms with many spectral components can be efficiently handled by the harmonic-balance technique coupled with Krylov-subspace methods. The paper extends this approach to the computation of the front-end noise figure in the presence of a strong interfering signal.

## INTRODUCTION

Microwave front-ends for modern telecommunications systems such as mobile radio consist of integrated analog or digital circuits of high topological complexity. In particular, thanks to the widespread use of MMIC and/or Silicon IC technology, traditional single-function circuits such as amplifiers or mixers tend to be merged into multifunctional blocks, the final objective being represented by the single-chip transceiver. Microwave CAD techniques must obviously catch up with this rapid technological advance in order to retain their traditional role of indispensable support to R&D engineering. This explains the quickly growing attention that is being devoted to nonlinear simulation techniques allowing large problems of several tens of thousands equations (or even more) to be efficiently tackled.

The extension of harmonic-balance (HB) analysis to large-size problems has been pursued by several authors. The proposed algorithms are normally based on the Newton-nodal HB approach [1], and rely on Krylov-subspace or other iterative methods for finding the Newton update at each step of the main iteration [2], [3]. This avoids the need for storing and factorizing the Jacobian matrix. As an alternative, the inexact-Newton harmonic balance (INHB) discussed in [4] makes use of the piecewise HB approach and of inexact Newton methods for solving the nonlinear system. With the INHB, only an approximate Newton update is computed at all but the last few steps, which considerably reduces the total number of matrix-vector multiplications [4]. In addition, the number of unknown waveforms equals the number of device ports, which is always significantly smaller than the number of circuit nodes. In this way the total number of equations is effectively minimized, and so is the memory required to store the basis vectors of the Krylov subspace.

In all cases, this class of methods has only been applied until now to the computation of the signal properties of RF/microwave front-ends. On the other hand, for system simulation purposes front-end noise is also of primary importance. The main objective of this paper is to extend the INHB technique to the noise analysis of large nonlinear RF/microwave circuits. Specifically, the task addressed in the paper is the computation of the front-end noise figure (NF) in the presence of an interfering signal of arbitrary strength. This problem is of primary importance especially in a personal and mobile communications environment, but to the authors' knowledge has not yet received a rigorous CAD-oriented solution. The results provide direct information on receiver sensitivity (including minimum detectable signal) and desensitization due to interference [5]. The problem is particularly demanding in terms of computer resources, since it requires a perturbative analysis of the quasi-periodic regime resulting from the intermodulation of the LO and interfering signals. Thus for large front-ends this kind of analysis cannot be afforded by ordinary nonlinear simulation techniques.

## FRONT-END NOISE FIGURE

We assume that both the local oscillator and the interferer are sinusoidal, with angular frequencies $\omega_{LO}$, $\omega_{INT}$, respectively. Similarly, the RF and IF frequencies will be denoted by $\omega_{RF}$, $\omega_{IF}$, respectively. In a highly polluted electromagnetic environment, the interferer may be larger than the useful RF signal by many orders of magnitude, and may even fall within the passband of the RF preselection filter. In such situations, the interferer may produce a degradation of the front-end noise performance by three different mechanisms. i) Since the interferer is relatively large, it may drive the small-signal preamplifier stages and/or the mixer (especially if active) into gain compression, which results in a drop of the receiver conversion gain, and in a noise figure increase. ii) All the noise components located at an offset $\pm\omega_{IF}$ from $\omega_{INT}$ will beat with the interferer in the device nonlinearities, and produce additional noise contributions superimposed on the down-converted (IF) carrier. iii) Reciprocally, the interferer noise components located at an offset $\pm\omega_{IF}$ from $\omega_{LO}$ will beat with the local oscillator, and will produce additional contributions to the IF noise [5]. Thus, assuming that noise power is very small, the noise calculations of interest require a first-order perturbation analysis of the *quasi-periodic* steady state [6] generated by the intermodulation of the (noiseless) LO and interferer signals. On the other hand, since the NF is a linear concept [7], the RF signal may be treated as a small perturbation of the same quasi-periodic regime.

The perturbative analysis of a quasi-periodic steady state was discussed in detail in [6], and will not be repeated here. For later convenience, we recall that in the vicinity of the steady state the nonlinear subnetwork may be described by a set of complex linear equations relating the vectors $\delta\mathbf{V}$, $\delta\mathbf{I}$, $\delta\mathbf{X}$ of all the perturbation phasors on voltages, currents, and state variables, at all the sidebands. This system takes on the form

$$\delta\mathbf{V} = \mathbf{P}\,\delta\mathbf{X} \quad ; \qquad \delta\mathbf{I} = \mathbf{Q}\,\delta\mathbf{X} \tag{1}$$

(1) are the conversion equations of the nonlinear subnetwork, and $\mathbf{P}$, $\mathbf{Q}$ are its (complex) conversion matrices of size $n_D n_S$, where $n_S$ is the total number of noise sidebands, and $n_D$ is the number of nonlinear subnetwork (device) ports.

0-7803-4471-5/98/$10.00 (c) 1998 IEEE

The noise sources to be considered in the analysis are those introduced by the nonlinear devices, by the linear subnetwork, by the local oscillator, and by the noise sidebands of the interfering signal. These contributions have different physical origins, and may thus be superimposed in power. Also, in each case the computational mechanism is pretty much the same, consisting in the combination of (1) with the linear subnetwork equations, with minor formal changes. Thus for the sake of brevity only the device noise will be discussed in detail. Irrespective of its physical origin, the noise generated by the active devices may be globally described by a set of $n_D$-vectors $\mathbf{J}_{hk}(\omega)$ whose entries are random phasors of pseudo-sinusoidal equivalent current sources at the device ports [8]. Specifically, $\mathbf{J}_{hk}(\omega)$ represents the noise components falling in a 1 Hz band located at an offset $\omega$ from the steady-state harmonic $\Omega_{hk}=h\omega_{LO}+k\omega_{INT}$. The $n_Dn_S$-vector obtained by stacking the $\mathbf{J}_{hk}(\omega)$ associated with all noise sidebands will be denoted by $\mathbf{J}(\omega)$. In order to carry out a spot noise analysis at a given frequency offset, we must evaluate the transfer of noise power from these current sources to the IF. For this purpose, we first represent the linear part of the front-end as an $(n_D + 1)$-port network $\mathcal{N}_L$. The first port of $\mathcal{N}_L$ (external port) represents the IF port, while the remaining $n_D$ ports are the ordinary linear subnetwork ports (device ports). The IF termination is included in $\mathcal{N}_L$. The high-frequency sources are also included in $\mathcal{N}_L$ together with their internal impedances, and their voltages are set to zero. We now stack the current and voltage phasors at the external port of $\mathcal{N}_L$ at all sidebands $\omega + \Omega_{hk}$ to build the vectors $\mathbf{I_E}$, $\mathbf{V_E}$ of dimension $n_S$. Similarly, the current and voltage phasors at the device ports are stacked into the vectors $\mathbf{I_D}$, $\mathbf{V_D}$ of dimension $n_Dn_S$. Taking as positive the currents entering the nonlinear subnetwork ports, the frequency-domain equations of $\mathcal{N}_L$ at all sidebands may be written in the matrix notation

$$\begin{bmatrix} \mathbf{I_E} \\ -\mathbf{I_D} \end{bmatrix} = \begin{bmatrix} \mathbf{Y_{EE}} & \mathbf{Y_{ED}} \\ \mathbf{Y_{DE}} & \mathbf{Y_{DD}} \end{bmatrix} \begin{bmatrix} \mathbf{V_E} \\ \mathbf{V_D} \end{bmatrix} \tag{2}$$

The nonlinear subnetwork may be replaced by a linear multifrequency circuit $\mathcal{N}_N$ representing its perturbative equivalent in the neighborhood of the quasi-periodic steady state. $\mathcal{N}_N$ is described by the conversion equations (1). This multiport has $n_S$ groups of $n_D$ ports, each corresponding to one of the sidebands. At each sideband, we now connect the device ports of $\mathcal{N}_L$ to the corresponding group of $n_D$ ports of $\mathcal{N}_N$ to obtain a linear multifrequency $n_S$-port network $\mathcal{N}$. By combining (1) with (2) we may express the $n_S$-vector of current phasors at the ports of $\mathcal{N}$ in the form

$$\mathbf{I_E} = -\mathbf{Y_{ED}}\,\mathbf{P}\,[\mathbf{Y_{DD}}\,\mathbf{P} + \mathbf{Q}]^{-1}\,\mathbf{J}(\omega) \tag{3}$$

Let the phasor of the pseudo-sinusoidal noise current flowing through the IF load at $\omega_{IF}$ be denoted by $\delta I_{IF}(\omega_{IF})$. Assuming that the noise sidebands are ordered in such a way that the IF be the first entry of $\mathbf{I_E}$, we may write

$$\delta I_{IF}(\omega_{IF}) = -\mathbf{R}\,\mathbf{Y_{ED}}\,\mathbf{P}\,[\mathbf{Y_{DD}}\,\mathbf{P} + \mathbf{Q}]^{-1}\,\mathbf{J}(\omega_{IF}) \triangleq -\mathbf{M}\,\mathbf{J}(\omega_{IF}) \tag{4}$$

where $\mathbf{R}$ is the 1 x $n_S$ row matrix $[1\ \ 0\ \ 0\ \ 0\ .....\ 0]$. The noise power delivered to the IF load resistance $R_{IF}$ in a 1-Hz band in the neighborhood of $\omega_{IF}$ (and originating from the device noise sources) is then given by

$$N_D(\omega_{IF}) = R_{IF} \langle|\delta I_{IF}(\omega_{IF})|^2\rangle = R_{IF}\,\mathbf{M} \langle \mathbf{J}(\omega_{IF})\,\mathbf{J}^{\dagger}(\omega_{IF})\rangle\,\mathbf{M}^{\dagger} \tag{5}$$

where $^{\dagger}$ denotes the conjugate transposed of a complex matrix, and $\langle\bullet\rangle$ denotes the ensemble average. The same kind of linearized analysis can be used to compute the conversion gain from $\omega_{RF}$ to $\omega_{IF}$, as well as the IF noise spectral densities originating from the linear subnetwork, the LO, and the interferer noise. These quantities will be denoted by $G_{Tc}(\omega_{IF})$, $N_{LS}(\omega_{IF})$, $N_{LO}(\omega_{IF})$, and $N_{INT}(\omega_{IF})$, respectively. Assuming that the circuit is held at a reference absolute temperature $T_0$, and that the IF termination is noiseless, the spot NF of the receiver is then given by [7]

$$F = \frac{N_D(\omega_{IF}) + N_{LS}(\omega_{IF}) + N_{LO}(\omega_{IF}) + N_{INT}(\omega_{IF})}{K_B\,T_0\,G_{Tc}(\omega_{IF})} \tag{6}$$

where $K_B$ is Boltzmann's constant. Let the RF impedance level of the receiver be denoted by $R_0$. The amplitude of the minimum detectable signal in a channel of bandwidth B is then given by [5]

$$V_{MDS} = \sqrt{8\,R_0\,K_B\,T_0\,F\,B} \tag{7}$$

## COMPUTATIONAL ASPECTS

The computation of the conversion matrix $\mathbf{M}$ by ordinary methods requires the storage and factorization of the complex matrix $\mathbf{Y_{DD}}\,\mathbf{P} + \mathbf{Q}$, whose dimension is $n_Dn_S$. This approach may soon become impractical even for front-ends of moderate size. As an example, consider a circuit containing about 100 transistors and requiring about 100 positive frequencies for an accurate HB analysis. In this case $n_D \approx n_S \approx 200$, so that the dimension of $\mathbf{Y_{DD}}\,\mathbf{P} + \mathbf{Q}$ is about 40000, corresponding to a real matrix of dimension 80000. Storing and handling a matrix of this size is definitely impractical even on large computer systems, not to mention that the size of many practical problems may be much larger than this [2].

In order to circumvent this difficulty, we analyze in detail the structure of $\mathbf{M}$ as defined by (4). We may write

$$\begin{aligned} \mathbf{M} &= \mathbf{R}\,\mathbf{Y_{ED}}\,\mathbf{P}\,[\mathbf{Y_{DD}}\,\mathbf{P} + \mathbf{Q}]^{-1} = \\ &= \{[(\mathbf{Y_{DD}}\,\mathbf{P} + \mathbf{Q})^{tr}]^{-1}\,(\mathbf{R}\,\mathbf{Y_{ED}}\,\mathbf{P})^{tr}\}^{tr} \triangleq \{\mathbf{A}^{-1}\,\mathbf{b}\}^{tr} \end{aligned} \tag{8}$$

where

$$\begin{aligned} \mathbf{A} &= (\mathbf{Y_{DD}}\,\mathbf{P} + \mathbf{Q})^{tr} = \mathbf{P}^{tr}\,\mathbf{Y_{DD}}^{tr} + \mathbf{Q}^{tr} \\ \mathbf{b} &= (\mathbf{R}\,\mathbf{Y_{ED}}\,\mathbf{P})^{tr} = \mathbf{P}^{tr}\,\mathbf{Y_{ED}}^{tr}\,\mathbf{R}^{tr} \end{aligned} \tag{9}$$

and $^{tr}$ denotes transposition. Thus $\mathbf{M}$ may be computed by solving with the GMRES method [9] or some other iterative procedure a large linear system of the canonical form $\mathbf{A}\ \mathbf{x} = \mathbf{b}$, with suitable preconditioning. The submatrices $\mathbf{Y_{RS}}$ (R, S = E, D) describe the linear subnetwork and are thus block-diagonal (different frequencies are uncoupled), each (square or rectangular) diagonal block being associated with a single noise sideband. These submatrices may thus be handled (i.e., stored and multiplied by other matrices) by ordinary methods without difficulty. Due to (9), the bulk of the computational effort required by a GMRES iteration [9] is then spent in performing matrix-vector products of the form

$$\mathbf{P}^{tr}\,\mathbf{g}\ \ ;\qquad \mathbf{Q}^{tr}\,\mathbf{g} \tag{10}$$

where $\mathbf{g}$ is a generic complex $n_Dn_S$-vector. On the other hand, $\mathbf{P}^{tr}$, $\mathbf{Q}^{tr}$ are sums of Toeplitz matrices [6], so that the products (10) may be expressed by means of discrete convolutions, and

may be evaluated by the fast Fourier transform [10]. This provides sufficient numerical efficiency for most applications, with a relatively slow (asymptotic) dependence on the number of sidebands of the form $n_S \log n_S$. Note that while **P**, **Q** cannot be stored in the computer memory because of their size, they can be re-computed with minimal effort each time they are needed, starting from a set of Fourier coefficients [6] that can be typically stored in a few Mbytes (e.g., see [4] and the example reported in the next section).

The last step of the noise analysis procedure is the computation of (5). The noise correlation matrix $<\mathbf{J}(\omega)\,\mathbf{J}^{\dagger}(\omega)>$ is formally a complex square matrix of dimension $n_D n_S$, which cannot be directly stored. However, it should be recalled that the nonlinear subnetwork is a collection of individual devices. Let the total number of devices be denoted by N, and the number of ports of the i-th device by $n_i$. Two noise sources belonging to distinct devices are statistically independent because of their different physical origins, so that their correlation is zero. On the other hand, the noise sideband sources belonging to a same device may be correlated [8]. The maximum number of nonzero entries of $<\mathbf{J}(\omega)\,\mathbf{J}^{\dagger}(\omega)>$ is thus given by

$$n_J = \sum_{i=1}^{N} (n_i n_S)^2 << (n_D\ n_S)^2 \qquad (11)$$

where the inequality is justified by the fact that for most devices $n_i$ is small (usually 1 or 2). Obviously only the nonzero elements are computed and stored, and the sparsity of the matrix is exploited in the computation of (5).

## AN EXAMPLE OF APPLICATION

Let us consider a typical single-conversion receiver front-end, whose functional diagram in terms of interconnected blocks is given in fig. 1. The circuit basically consists of two doubly balanced mixers arranged in an image-rejection configuration, plus coupling networks, amplifiers, and filters. The band of operation is 935 - 960 MHz with a fixed IF of 90 MHz. The passband of the RF preselection filter coincides with the front-end band, and its attenuation at 900 MHz is about 30 dB. The circuit-level description of the front-end is very detailed, and includes many (linear) parasitic components. The total number of device ports is $n_D = 208$, and the total number of nodes is 1745. The front-end is analyzed as a single circuit, so that inter-block couplings that may exist for various reasons such as imperfect isolation or proximity effects may be accounted for without difficulty. The far-from-carrier noise spectral densities of both the LO and the interferer are assumed equal to -150 dBc/Hz.

Fig. 2 shows the front-end conversion gain as a function of the power level of a 915 MHz interfering tone, with 0 dBm LO power and $\omega_{RF} = 2\pi \cdot 947.5$ MHz (corresponding to center band). This curve is obtained by frequency-conversion analysis of the two-tone quasi-periodic regime generated by the intermodulation of the LO and interferer signals. The quasi-periodic regime is computed by INHB analysis with IM products of the two exciting tones up to the 9th order. The total number of positive frequencies of the steady state is thus 90, and the total number of INHB unknowns is 37648. This corresponds to a nodal HB problem of 315845 unknowns. The average CPU time required for the nonlinear analysis is about 1860 seconds per power point on a SUN Ultra 2 workstation. The number of sidebands is $n_S = 181$, so that each frequency-conversion analysis requires the solution of a real system of 75296 equations (631690 nodal equations), and takes about 249 seconds. The interferer power is swept from -70 dBm in 5 dB steps up to a very high level (in a relative sense) of +5 dBm, corresponding to over 25 dB gain compression, in order to demonstrate the excellent power-handling capabilities of the INHB algorithm.

Fig. 3 shows the total front-end NF as a function of the power level of the interfering tone. The different contributions to the NF as defined by (6) are also shown in this figure. The results may be explained as follows. The LO contribution is practically zero due to the assumption of perfectly balanced mixer topologies. At low levels of interference only the internal mixer noise is significant and the conversion gain is flat, so that the NF is also flat. Above a certain level of interference, the receveir gain starts to compress according to fig. 2, so that the NF starts to increase due to (6). Note, however, that a compression effect is observed on all conversion coefficients, so that the internal noise $N_D(\omega_{IF}) + N_{LS}(\omega_{IF})$ is a decreasing function of the interferer power. Thus the growth of the internal noise contribution to the receiver NF is less rapid than the gain drop. On the other hand, the interferer noise contribution grows linearly with the interferer power because the noise sideband relative level remains constant (at -150 dBc/Hz in the present case). Thus the interferer noise may also become significant (as in fig. 3) above some level of interference. The CPU time for a noise analysis is about 838 seconds on a SUN Ultra 2 workstation.

Fig. 4 shows the amplitude of the minimum detectable signal (in μV) under the same conditions, as obtained from (7) with B = 200 kHz and $R_0 = R_{IF} = 50\ \Omega$. Finally, in fig. 5 the receiver NF and the minimum detectable signal are plotted against the distance between the interfering transmitter and the receiver, under the assumptions of 1 W radiated power at 915 MHz, matched half-wave dipole antennas, and free-space propagation.

The total memory occupation of the program is about 442 MB. The memory required to store the Fourier coefficients for the computation of **P** and **Q** is about 9 MB, and the memory required to store the nonzero entries of the noise correlation matrix $<\mathbf{J}(\omega)\,\mathbf{J}^{\dagger}(\omega)>$ is about 2 MB.

## ACKNOWLEDGMENTS

This work was partly sponsored by the Italian Ministry of University and Scientific Research (MURST) and by the Istituto Superiore delle Comunicazioni e delle Tecnologie dell' Informazione (ISCTI).

## REFERENCES

[1] K. S. Kundert and A. Sangiovanni-Vincentelli, "Simulation of nonlinear circuits in the frequency domain", *IEEE Trans. Computer-Aided Design*, Vol. CAD-5, Oct. 1986, pp. 521-535.

[2] R. C. Melville, P. Feldmann, and J. Roychowdhury, "Efficient multi-tone distortion analysis of analog integrated circuits", *1995 IEEE Custom Int. Circuits Conf. Digest*, May 1995, pp. 241-244.

[3] M. M. Gourary *et al.*, "Iterative solution of linear systems in harmonic balance analysis", *1997 IEEE MTT-S Int. Microwave Symp. Digest*, Denver, CO, June 1997, pp. 1507-1510.

[4] V. Rizzoli *et al.*, "Fast and robust inexact-Newton approach to the harmonic-balance analysis of nonlinear microwave circuits", *IEEE Microwave Guided Waves Lett.*, Vol. 7, Oct. 1997, pp. 359-361.

[5] U. L. Rohde, J. Whitaker, and T. T. N. Bucher, *Communications Receivers (second edition)*. McGraw-Hill: New York, 1997.

[6] V. Rizzoli, D. Masotti, and F. Mastri, "Full nonlinear noise analysis of microwave mixers", *1994 IEEE MTT-S Int. Microwave Symp. Digest*, San Diego, CA, May 1994, pp. 961-964.

[7] S. A. Maas, *Microwave Mixers (second edition).* Artech House: Norwood, 1993.

[8] V. Rizzoli, F. Mastri, and D. Masotti, "General noise analysis of nonlinear microwave circuits by the piecewise harmonic-balance technique", *IEEE Trans. Microwave Theory Tech.*, Vol. 42, May 1994, pp. 807-819.

[9] Y. Saad and M. H. Schultz, "GMRES: a generalized minimal residual method for solving nonsymmetric linear systems", *SIAM J. Sci. Stat. Comput*, Vol. 7, July 1986, pp. 856-869.

[10] H. J. Nussbaumer, *Fast Fourier Transform and Convolution Algorithms*. Springer-Verlag: Berlin, 1981.

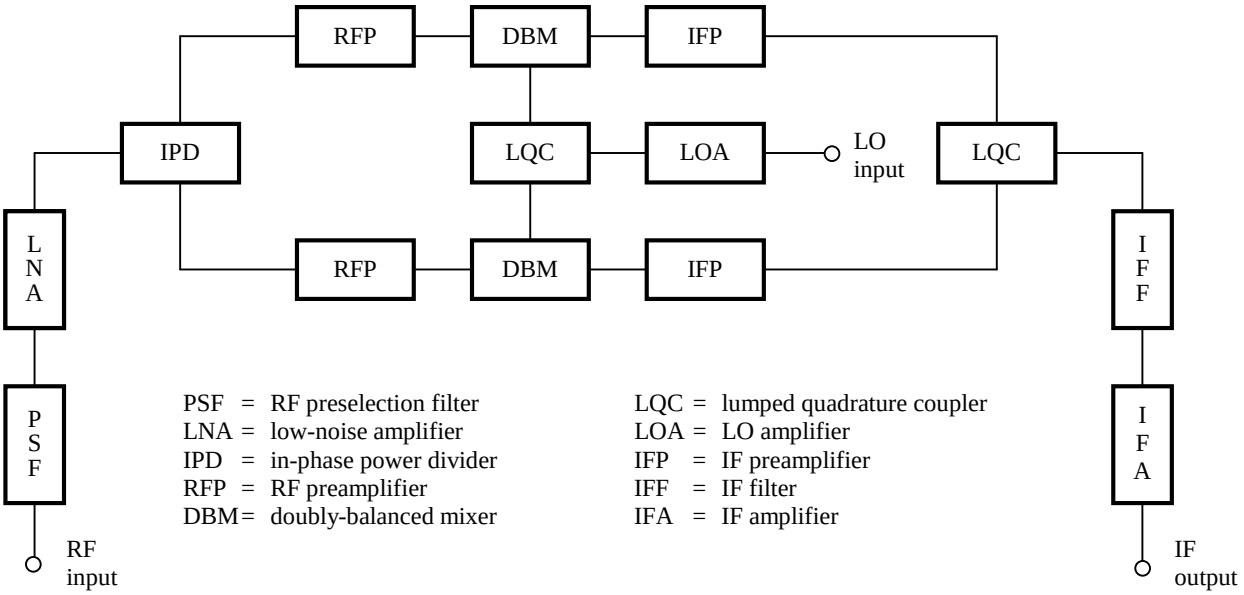


Fig. 1 - Schematic topology of a microwave front-end.

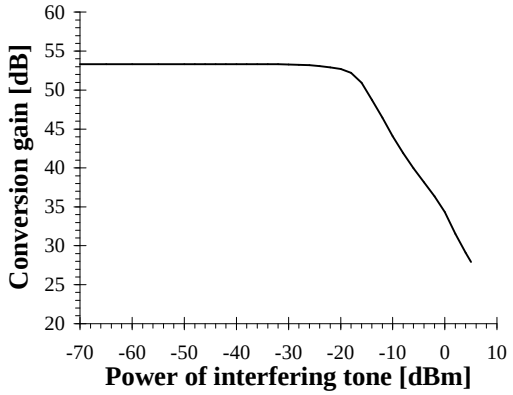


Fig. 2 - Conversion gain in the presence of interference.

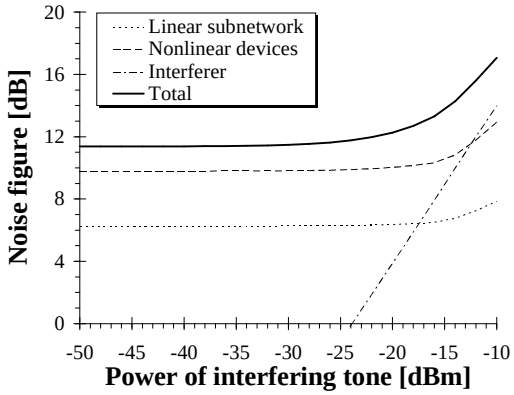


Fig. 3 - Noise figure in the presence of interference.

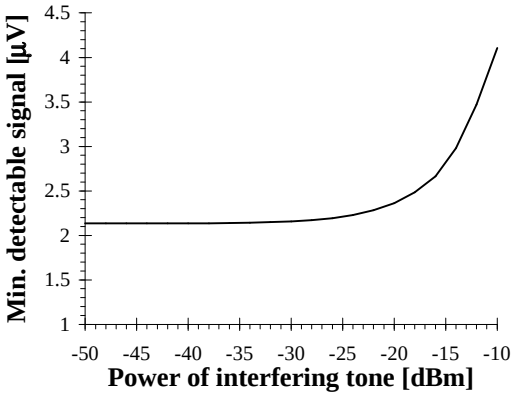


Fig. 4 - Minimum detectable signal in the presence of interference.

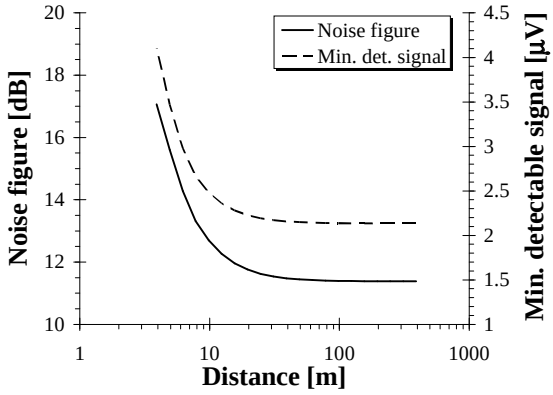


Fig. 5 - Effects of distance from source of interference.